SAND2011-2566C

Radar Cross Section Statistics of Dismounts at Ku-band

Ann Marie Raynal*[a], Bryan L. Burns[a], Tobias J. Verge[b], Douglas L. Bickel[a], Ralf Dunkel[b], Armin W. Doerry[a]
[a]Sandia National Laboratories, PO Box 5800, Albuquerque, NM, USA 87185-0519;
[b]General Atomics Aeronautical Systems Inc., Reconnaissance Systems Group, 13322 Evening Creek Drive North, San Diego, CA 92128, USA

ABSTRACT

Knowing the statistical characteristics of a target's radar cross-section (RCS) is crucial to the success of radar target detection algorithms. A wide range of applications currently exist for dismount (i.e. human body) detection and monitoring using ground-moving target indication (GMTI) radar systems. Dismounts are particularly challenging to detect. Their RCS is orders of magnitude lower than traditional GMTI targets, such as vehicles. Their velocity of about 0 to 1.5 m/s is also much slower than vehicular targets. Studies regarding the statistical nature of the RCS of dismounts focus primarily on simulations or very limited empirical data at specific frequencies. This paper seeks to enhance the existing body of work on dismount RCS statistics at Ku-band, which is currently lacking, and has become an important band for such remote sensing applications. We examine the RCS probability distributions of different sized humans in various stances, across aspect and elevation angle, for horizontal (HH) and vertical (VV) transmit/receive polarizations, and at diverse resolutions, using experimental data collected at Ku-band. We further fit Swerling target models to the RCS distributions and suggest appropriate detection thresholds for dismounts in this band.

Keywords: RCS, radar cross section, RCS distribution, RCS statistics, GMTI, DMTI, dismount RCS, human RCS

1. INTRODUCTION

The detection of dismounts, or human bodies, has become increasingly important for GMTI applications in recent years for border, facility, and battlefield monitoring of friends and foes. Humans are inherently mobile targets with a variable scattering return and non-linear phase response. Additionally, humans have a much lower radar cross section and slower motion than more traditional ground targets such as vehicles. These factors make the detection of dismounts in a real-world clutter environment quite challenging for radar and thus provide the motivation to understand the statistical nature of the RCS of dismounts for adequate detection.

An examination of the published literature yields some information on dismount RCS statistics in the Ku radiolocation band. However, most of the literature is based on electromagnetic simulations or limited empirical data. We performed three different RCS experiments of dismounts at Ku-band with three different calibrated test-bed radars. Our goal was to directly measure the RCS of dismounts with varying size, stance, pose relative to the radar, clutter, and polarization in order to observe the statistical characteristics of their RCS. We further examined RCS differences with resolution by signal processing of the data sets. Through these studies we hope to augment the existing literature on empirical dismount RCS statistics for improved detection and provide comparisons to the current simulation literature.

This paper is organized into four main parts. A review of the current literature on RCS statistics at Ku-band is provided in Section 2. A description of experiments conducted to find direct measurements of dismount RCS as a function of size, stance, pose, polarization, and clutter are outlined in Section 3. Experimental results regarding RCS distributions, statistics, and Swerling target models for 4-inch and 3-foot resolution are given in Section 4. Conclusions are made in Section 5.

*amrayna@sandia.gov; phone 1 505 284-3053; fax 1 505 844-0858; www.sandia.gov

2. REVIEW OF THE STATE-OF-THE-ART

The Army Research Laboratory (ARL) has published several findings about dismounts based primarily on electromagnetic modeling simulations. Le and Dogaru

[**1** for instance, report on Xpatch modeling of the human body at several frequencies. At Ku-band, their results show that the median RCS decreases with increasing grazing angle from 0 to 60 degrees by about 9dBsm for VV polarization and 5 dBsm for HH polarization. Due to ground bounce, HH polarization demonstrates significant advantage over VV polarization, particularly at higher grazing angles (e.g. a 4 dBsm increase at 15 degrees). The range of RCS values at Ku-band for VV is between −13 dBsm and 0 dBsm, with a -8.2 dBsm median and a 2.6 dBsm standard deviation at 30-degree grazing. Additionally, their data shows a clear trend of higher RCS with front and rear views, as one might expect due to the increased physical surface area of the human. The authors also conclude that RCS value does not change much with frequency.

Dogaru, et al.[**2**, further report on finite difference, time domain RCS results of both a fit and fat man model. The models are articulated into diverse postures (such as standing, kneeling, shooting, running, arms spread, etc.) from L to X-band. The average RCS of a 360-degree aspect view of a dismount at 0 degree grazing angle is demonstrated as independent of body posture and shape because scattering occurs principally from the trunk of the human rather than limb positioning. The authors note that body size is possibly more influential on average RCS, though they do not pursue this particular study. Measurements by Otero[**3** confirm that the human torso dominates RCS over all appendages combined, by a factor of 3 to 4 times. ARL's[**4** investigations of simulated micro-Doppler (returns from body appendages) of human movement show that the torso has a constant non-fluctuating RCS, in contrast to the limbs, as a dismount moves.

Analysis of simulated polarization effects[2] show that HH and VV polarizations are similar in response when a dismount is taken to be in free space. However, with the addition of a ground plane, VV polarization increases in RCS after about 30 degrees of grazing angle and HH polarization does so at all grazing angles due to ground bounce. As a function of aspect angle, a stronger return is evident from the backside of the dismount for all postures because of specular reflection from the flat surface. This effect is true irrespective of a ground plane, but is further enhanced for HH polarization with a ground plane present.

The impact of a dismount carrying a device to the overall RCS has also briefly been studied in the literature, though not at Ku-band. Stratton and Bender[**5** report on experimental RCS measurements at Ka-band and full polarimetry of a dismount standing, prone, and kneeling on absorber material with and without a grenade launcher. The experiment is over three grazing angles (2, 5, and 15 degrees) and four aspect angles of a quarter circle about the launcher. The mean RCS ranges from -15 to -4.3 dBsm for all grazing and aspect angles when the grenade launcher is held. The mean RCS decreases as the dismount changes posture, from standing to kneeling to prone, as well as when the launcher is absent. In addition, a simulation study[2] of a human carrying a large metal stick shows that VV polarization return is enhanced if the stick orientation is optimal for the flash at the particular grazing angle, but otherwise cross-polarizations more easily identify a weapon at the expense of overall lower RCS return.

A limited amount of literature comments on the Swerling target models of the dismount RCS distributions. Dogaru, et al.[2] state that the distributions of the fat man model standing and kneeling at L-band frequencies transition from Swerling 3 to Swerling 1 target models within the band. Hersey, et al.[**6** discuss dismount modeling and detection from unmanned aerial vehicles, wherein the RCS distribution of their dismount kinematic model shows Swerling 3 target characteristics for a walking human at X-band. That is, the dismount is composed of multiple scatterers with one being dominant and fluctuations occurring in slow time (i.e. per scan).

3. DISMOUNT RCS EXPERIMENTS

The three dismount RCS experiments that we conducted at Ku-band are described next. In all cases, we acquired the RCS of stationary dismounts using synthetic aperture radar (SAR) under the assumptions that results are applicable to GMTI because the RCS of the torso is the principal contributor to the total RCS and is constant irrespective of the dismount's motion, according to the aforementioned results.

[**3**, [**4**

3.1. Experiment #1: Vertical Polarization, Size, Stance, and Pose

Experiment #1 consisted of examining the RCS of dismounts as a function of size, stance, pose, and vertical polarization for a single grazing angle and all aspect angles. Three subjects were used for the experiment: a large, medium, and small person, with weights and heights as in Table 1.

Table 1. Experimental Subject Height and Weight

	Small	Medium	Large
Height (ft, in.)	5'4-inch	5'8"	6'
Weight (lbs)	110	160	220

Four SAR spotlight mode circle passes were executed about the test site. Images were acquired every 12 degrees at a grazing angle of 18 degrees and a resolution of 4 inches at Ku-band with vertical polarization. Calibrator quad corner reflectors were placed in the scene to obtain absolute RCS. A cherry picker with a mounted video camera filmed the test execution. The subjects were asked to alternate stances and location in the target scene for each pass, while always facing true north and remaining as still as possible. The stances tested were sitting, kneeling, and standing. Standing also involved cases of holding or not holding a semi-automatic rifle. The target scene, personnel locations, and stances for each pass can be noted in Table 2 and Figure 1.

Table 2. Experimental Subject, Stance, and Location for Spotlight Circle Mode Collects

Circle Pass	Location 1	Location 2	Location 3	Location 4
A	Vacant	Small/Rifle	Medium/Standing	Large/Kneeling
B	Vacant	Medium/Rifle	Large/Standing	Small/Kneeling
C	Vacant	Large/Rifle	Small/Standing	Medium/Kneeling
D	Medium/Sitting	Large/Sitting	Small/Sitting	Vacant

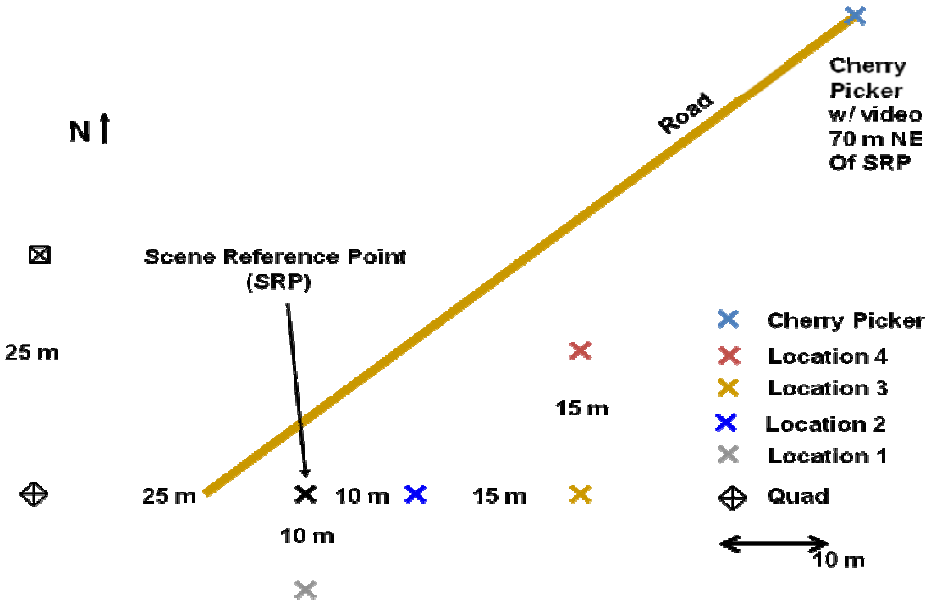

Figure 1. Experimental Setup of Target Scene

More specifically, the small person sat with legs crossed; knelt on one knee; and held the rifle in a shooting position. The medium person sat with legs crossed; knelt on both knees and haunches; and held the rifle in both hands in a front carry position. The large person sat with legs outstretched and open, with arms flung back; knelt on both knees; and held the rifle with one hand in a side carry position. All subjects stood with arms at their sides when not holding the rifle. Images of these stances from the video camera can be seen in Table 3. Note also from the table that the clutter background was

desert sand and vegetation for this experiment. Although different clutter backgrounds may impact the range of variation of the RCS, this parameter space was not explored in this test, except insofar as the subjects changing location amidst the same clutter type.

Table 3. Specific Experimental Subject Stances

Subject	Sitting	Kneeling	Standing	Rifle
Small				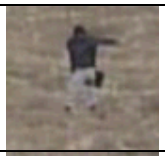
Medium			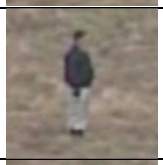	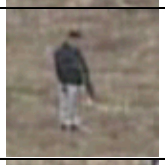
Large				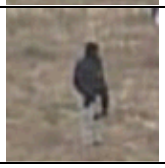

3.2. Experiment #2: Vertical Polarization, Size, Pose, and Different Clutter

The second experiment consisted of examining the RCS of dismounts as a function of size and pose for multiple grazing angles and aspect angles with vertical polarization in a different clutter environment. Four subjects were used for the experiment: one large, one medium, and two small persons. Five synthetic aperture radar spotlight passes were executed about the test site, whereby the platform flew a straight line back and forth while focusing on a reference point on the ground with squinted geometry spanning 90 degrees. With this type of flight collection geometry, the grazing angle changes as a function of the platform trajectory and squint angle as shown in

Figure 2. Note that the amount of variation in the grazing angle within the aperture increases as the grazing angle becomes steeper. Images were acquired roughly every 10 degrees in azimuth, with a grazing angle at the center of the pass of 7, 18, and 35 degrees, and a resolution of 4 inches at Ku-band with vertical polarization. The 7 and 18 degree passes covered 90 degrees in aspect of the subjects (front to side). Two passes at 35 degrees covered 180 degrees in aspect of the subjects (front to back). A spherical calibrator was placed at the scene center to obtain absolute RCS. The

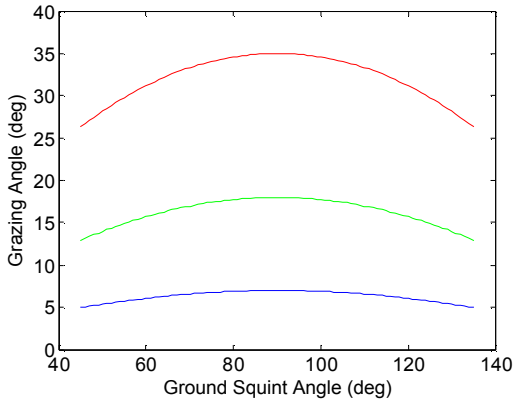

subjects were asked to stand in the scene for each pass and remain as still as possible. The target scene and personnel locations for each pass can be noted in Figure 3. Desert clutter of cracked, dry dirt and large, sparsely located, shrubs were at the target scene, as noted in Figure 3.

Figure 2. Variation in Grazing Angle with Squint

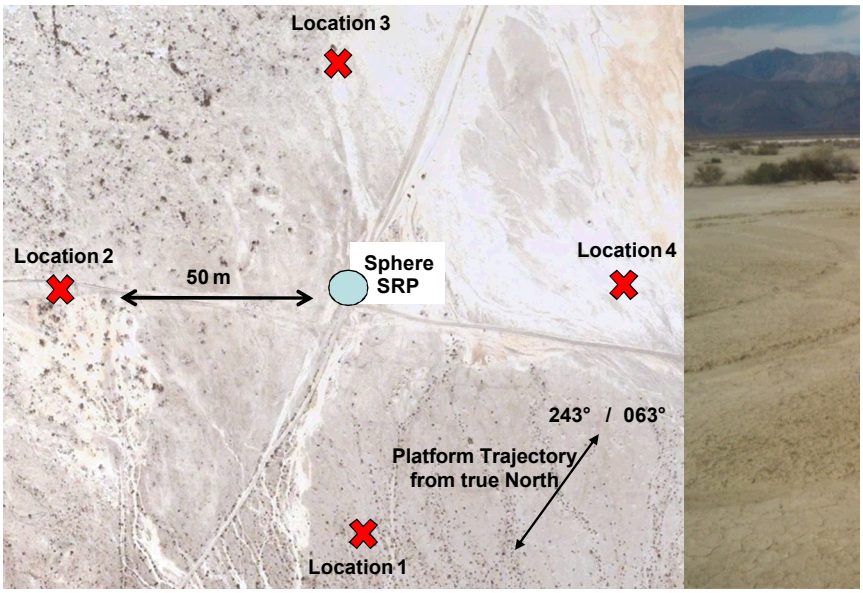

Figure 3. Grazing Angle Experiment Target Scene

3.3. Experiment #3: Horizontal Polarization, Size, and Pose

Experiment #3 consisted of examining the RCS of dismounts as a function of size and pose for a single grazing angle and all aspect angles with horizontal polarization. Four subjects were used for the experiment: two large, one medium, and one small person. Three synthetic aperture radar spotlight circle passes were flown. Images were acquired every 10 degrees in azimuth, with a grazing angle of 35 degrees and a resolution of 4 inches at Ku-band with horizontal polarization. This test was conducted at Sandia's radar calibration site as shown in Figure 4 to obtain absolute RCS. The subjects were asked to stand in the scene, facing true north for each pass and remaining as still as possible. The scene clutter was desert with vegetation as in the first experiment.

4. DISMOUNT RCS EXPERIMENTAL RESULTS

The human dismount RCS measurements described in the prior section are analyzed next.

4.1. Typical SAR Image Chip of a Dismount

Figure 5 shows a typical SAR image chip for a dismount from the data set of Experiment #1. The dismount is distinguished by a bright backscatter return at the location of the dismount with Doppler spreading due to the fact that the subjects do not remain perfectly still. The shadow of the dismount is also visible. The desert background clutter is noticeable throughout the image chip as well.

4.2. Dismount RCS Distribution and Statistics Methodology

We assumed a peak detection algorithm for our dismount RCS measurements. The maximum RCS pixel value in dBsm of each dismount's backscatter return (marked by the red X in Figure 5) was selected and compiled to generate a probability density function (PDF). The PDF was then integrated numerically to find the cumulative distribution function (CDF) for the data set. We further generated a PDF of the normalized clutter reflectivity in the experiments and noted the clutter mean to ensure sufficient differentiation from the dismount RCS values. We extracted several statistics from our results: 1) the geometric or logarithmic average, 2) the standard deviation of the PDF, 3) the arithmetic or linear average, 4) the median, estimated from the CDF where the probability is 0.5, and 5) the distribution dynamic range, estimated in

the following manner. We fitted the Swerling 1 (no dominant scatter, pulse-to-pulse correlation) and Swerling 3 (dominant scatterer, pulse-to-pulse correlation) models

[**7** with the following equations against our PDFs in order to determine the Swerling type:

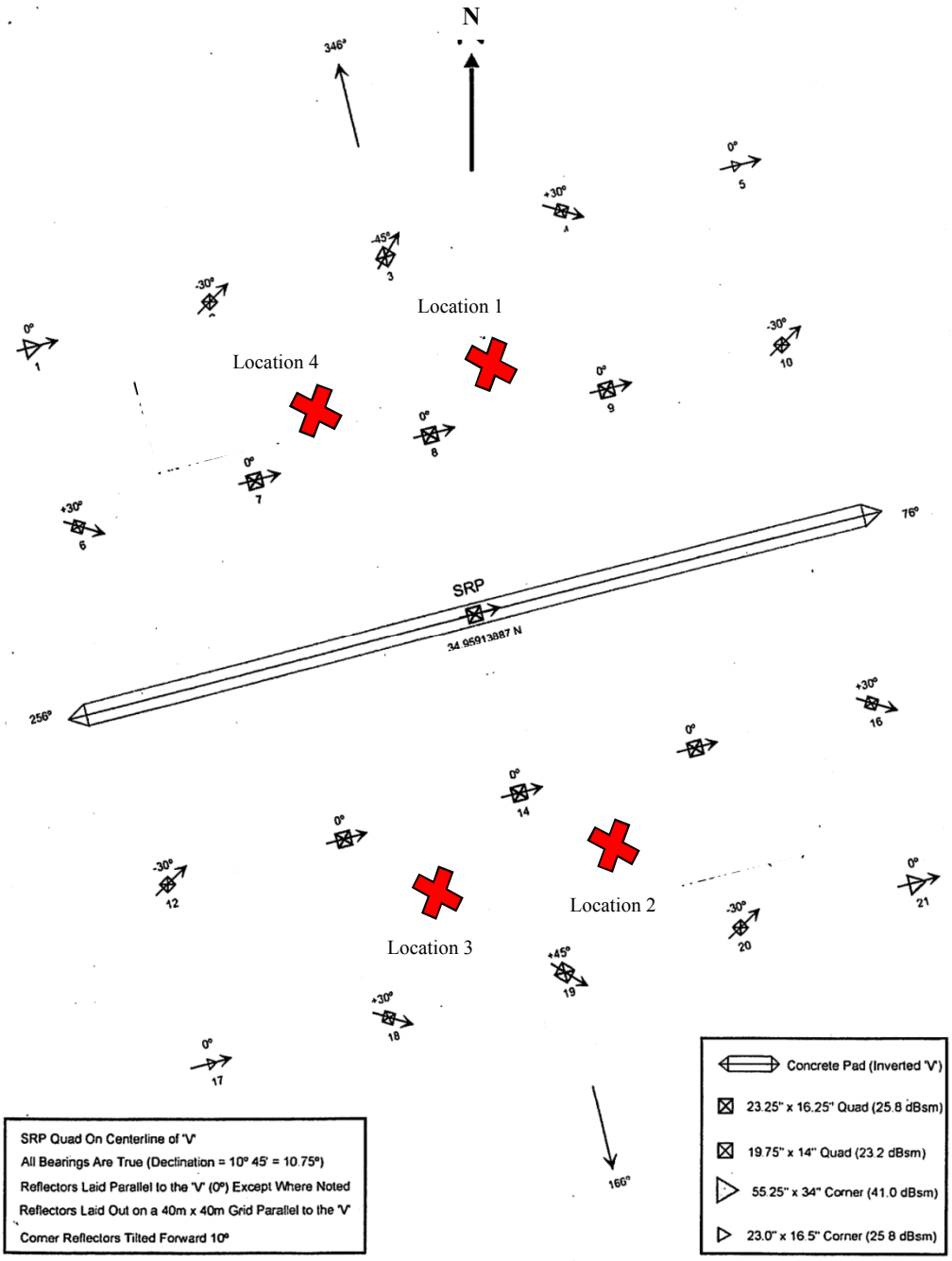

Figure 4. Horizontal Polarization Experiment Target Scene

$$f_{\text{Swerling\_1}}(\sigma) = \frac{1}{\sigma_{\text{avg}}} e^{-\frac{\sigma}{\sigma_{\text{avg}}}} \quad \text{and} \quad f_{\text{Swerling\_3}}(\sigma) = \frac{4\sigma}{\sigma_{\text{avg}}^2} e^{-\frac{2\sigma}{\sigma_{\text{avg}}}},$$

where σ is the actual or instantaneous RCS, σ_{avg} is the average linear RCS of the target over all fluctuations, and $f_{\text{Swerling\_\#}}$ is the chi-square PDF of 2 or 4 degrees for Swerling 1 or 3 targets, respectively. We then captured the minimum RCS threshold and dynamic range required for probabilities of 0.9 to 0.1 for a Swerling 3 target (which it turns out is the model for the distributions) by determining that $\sigma \geq \sigma_{avg}\beta$, where $\beta = -5.8$ or 2.9 dBsm using:

$$P_{\text{Swerling\_3,4}}\left\{\frac{\sigma}{\sigma_{\text{avg}}} \geq \beta\right\} = (1+2\beta)e^{-2\beta}$$

.

We additionally investigated the probability distributions of dismounts at a coarser resolution of 3 feet or about 1 meter by windowing our 4-inch resolution data and calibrating the RCS using the brightest corner reflector response in the scene. The return of the dismount was confined to a smaller number of resolution cells through this process.

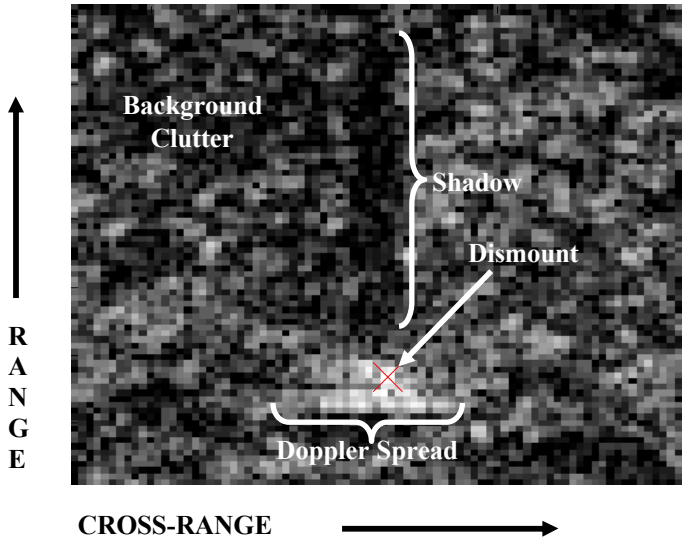

Figure 5. Representative SAR Image Chip of a Dismount (X=Peak RCS Pixel)

4.3. Clutter Distributions for All Experiments

The normalized reflectivity probability distribution of the clutter background at an arbitrary representative reference point in the images is plotted in

Figure 6 for all experiments. The clutter RCS is Gaussian-distributed with a geometric mean and corresponding normalized reflectivity as noted in parentheses, respectively. Experiment #2 had the brightest clutter background, and Experiment #1 the lowest. Experiment #3 had a relatively low clutter background, similar to Experiment #1 because the clutter types were similar. All experiments had clutter distinguishable from the dismounts.

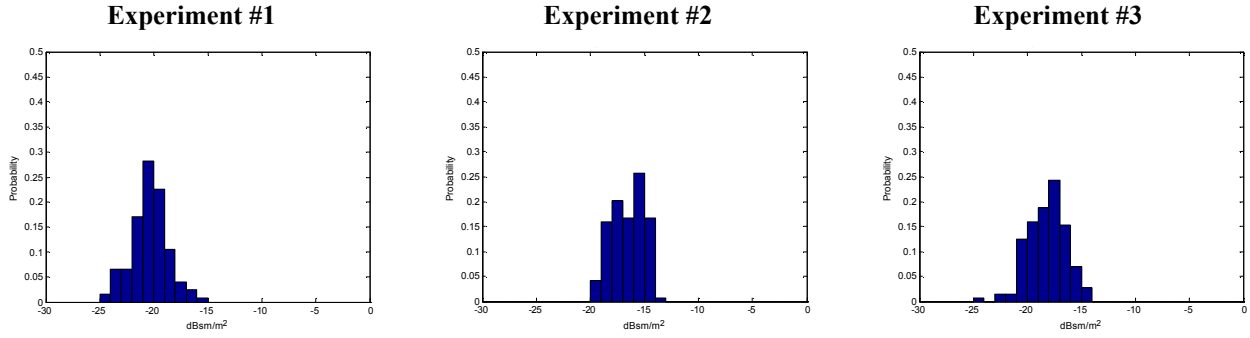

(-40.1 dBsm, -20.4 dBsm/m^2) (-23.8 dBsm, -4.5 dBsm/m^2) (-36.9 dBsm, -18.1 dBsm/m^2)

Figure 6. Normalized Reflectivity PDF of Clutter for All Experiments with (Geometric Mean, Normalized Reflectivity)

4.4. Dismount Distributions and Statistics for All Experiments

Figure 7 shows the overall dismount RCS statistics, PDFs, and CDFs for each experiment at 4-inch resolution. The overall results for all experiments are included, as well as the 35-degree grazing angle, VV results of experiment #2 for comparison to experiment #3's collect at the same angle with HH polarization. Additionally, the overall results at 3-foot resolution by coarsening of the 4-inch data set are included. The scales on all distributions are the same across results: -30 to 0 for the RCS in dBsm, 0 to 0.3 for the probability, and 0 to 1 for the cumulative probability. The 3-foot resolution results are the only exception, as their range is from -20 to 10 for the RCS values. In general, the RCS distributions and statistics are quite similar. We will proceed to analyze them in greater detail in the next sections.

4.5. Effects of Size, Stance, and Devices on Dismount Distributions

The statistical characteristics of the dismount remain fairly consistent irrespective of stance, size, and device. Figure 8 breaks down the dismount distributions of experiment #1 by size and stance for those postures without a rifle.

Figure 9 shows the dismount distributions for postures with a rifle. Those results are broken down by size for all stances without a rifle, those with a rifle, and all stances overall. All scales in the plots are as before. The number of samples for a single subject and stance pairing is 30, which is admittedly low and caution should be exercised with interpretation of results.

Notwithstanding, there does not appear to be a stark distinction between the distributions of stance, except for the medium-sized subject who produces a stronger backscatter return kneeling and sitting, as compared to standing by about 2-4 dBsm. In addition, the large and small subjects tend to have similar statistics, as compared to the medium-sized subject who has a 1-2 dBsm distribution shift towards higher RCS. These differences between the medium-sized subject and the other two subjects may be due to the fact that the individual had a greater width, as can be noted in the photographs of Table 3. We suspect that he produces a much stronger spherical versus cylindrical return as a result, in particular in the sitting and kneeling stances which accentuate his rotundity. In fact, based on height and weight ratio charts, the small subject was underweight, the large subject was overweight, and the medium subject was average in weight. Therefore, the height and weight ratio is unimportant in comparison with the distribution of weight on the dismount's body. This was also noticed in experiment #3, whereby the two large dismounts were of similar height and weight but one was much wider at the midsection, causing the subject's RCS to shift by roughly 1-2 dBsm. The other large dismount had RCS statistics comparable to the medium and small subjects. However, the shifts due to wider subjects are within one standard deviation of the mean and therefore of little statistical impact. The consistency in distributions and statistics across size and stance held true for experiment #2 as well.

A 1-2 dBsm distribution shift towards lower RCS seems to occur for all subjects when they are holding a rifle. Upon closer examination, the statistics of the small and medium-sized subjects with a rifle seem to be similar to those of them standing, which might be expected at non-flash angles of the rifle. This observation does not hold for the large subject, who was more mobile during the test while he was carrying a rifle and therefore had a larger Doppler spread of backscattered energy. Stratton, et al. in their studies of a dismount holding a rocket-propelled grenade launcher at Ka-band[**5**] suggest a dismount mean RCS of about -14dBsm, except at the flash aspect angle for a grazing angle of 15 degrees. This value is consistent with our observations.

Figure 10 confirms our observations by summarizing the geometric and arithmetic means, median, standard deviation, maximum, and minimum values of the probability distributions for all size, stance, and device permutations of experiment #1.

4.6. Effects of Aspect on Dismount Distributions

Figure 11 shows the variation in the mean RCS value in dBsm as a function of aspect angle of experiment #1, for lack of statistically significant data for a distribution. Zero degrees corresponds to true North or the front side of the human according to our collect. We note that the mean RCS variation is subtle as a function of aspect angle (i.e. no more than 2-3 dBsm). Granted, we do not have data at every angle nor in large samples because the center aperture angle of our circle

pass collects occur only every 12 degrees. Therefore caution must be exercised in making concrete conclusions about the RCS of the human as a function of aspect angle from this data.

4.7. Effects of Resolution on Dismount RCS Distribution

The PDF and CDF at 3-foot resolution, as well as their statistics, are approximately 6-7 dBsm stronger than the 4-inch resolution data for all experiments according to Figure 7. However, the PDF spread has a similar standard deviation of +/-3 dBsm for either resolution. The CDF shows this trend by means of the similar slope between the two cases as well.

Statistics	PDF	CDF
Experiment #1 (18º Grazing; VV; Many Stances, Sizes, Device, Aspects; 4" Resolution) Log Mean: -10.6 dBsm Arithmetic Mean: -9.3 dBsm Median: -11.8 dBsm Std. Dev.: 3.4 dBsm Range(0.1>P<0.9): -15.1 to -6.4 dBsm Swerling Target: 3	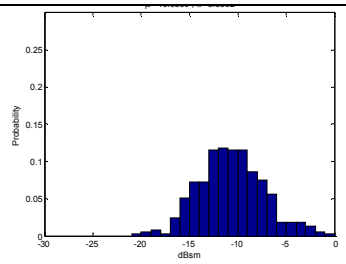	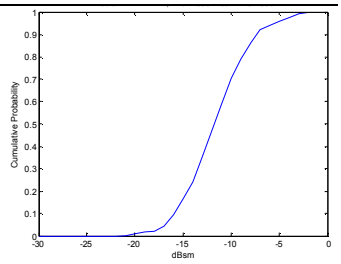
Experiment #2 (Many Grazing; VV; Standing; Many Sizes; Limited Aspect; 4" Resolution) Log Mean: -10.2 dBsm Arithmetic Mean: -9.8 dBsm Median: -11 dBsm Std. Dev.: 1.8 dBsm Range(0.1>P<0.9): -15.6 to -6.9 dBsm Swerling Target: 3	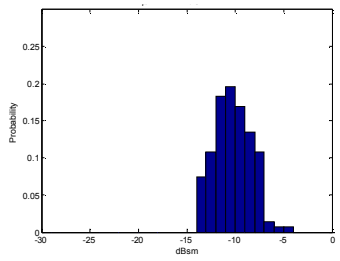	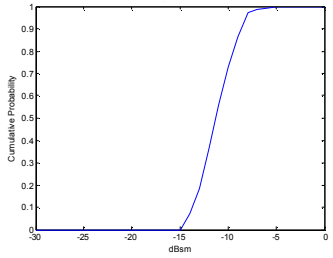
Experiment #3 (35º Grazing; HH; Standing; Many Sizes, Aspects, 4" Resolution) Log Mean: -11.6 dBsm Arithmetic Mean: -10.6 dBsm Median: -12.4 dBsm Std. Dev.: 2.9 dBsm Range(0.1>P<0.9): -16.4 to -7.7 dBsm Swerling Target: 3	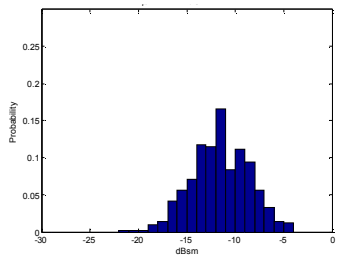	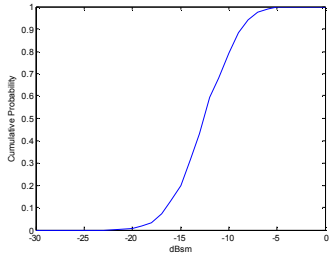
Experiment #2 (35º Grazing ONLY; VV; Standing; Many Sizes; Limited Aspect; 4" Resolution) Log Mean: -11.2 dBsm Arithmetic Mean: -10.9 dBsm Median: -12 dBsm Std. Dev.: 1.4 dBsm Range(0.1>P<0.9): -16.7 to -8 dBsm Swerling Target: 3	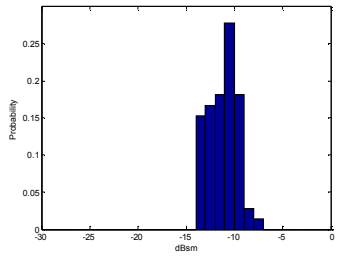	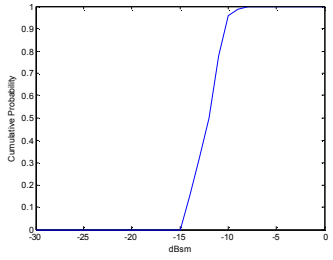
Overall (Experiments #1 to #3 -- Many Grazing, Polarization, Stances, Sizes, Device, Aspects, & Clutter, 4" Resolution) Log Mean: -11 dBsm Arithmetic Mean: -9.9 dBsm Median: -12.1 dBsm Std. Dev.: 3 dBsm Range(0.1>P<0.9): -15.7 to -7 dBsm Swerling Target: 3	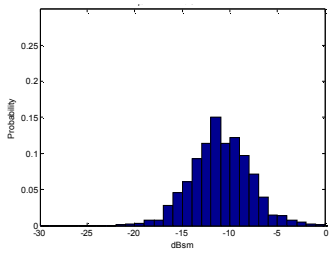	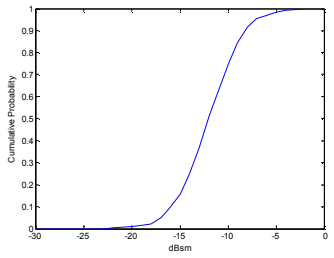

Overall (Experiments #1 to #3 -- Many Grazing, Polarization, Stances, Sizes, Device, Aspects, & Clutter, 3' Resolution)

```
Log Mean:  -4.8 dBsm
Arithmetic Mean:  -3.4 dBsm
Median:  -6.1 dBsm
Std. Dev.:  3.2 dBsm
Range(0.1>P<0.9):  -9.2 to -0.5 dBsm
Swerling Target:  3
```

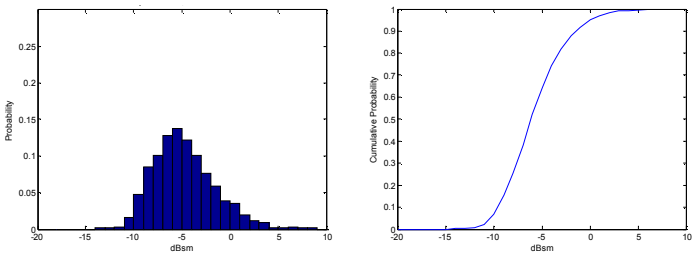

Figure 7. Dismount RCS Statistics, PDF, and CDF Summary for All Experiments

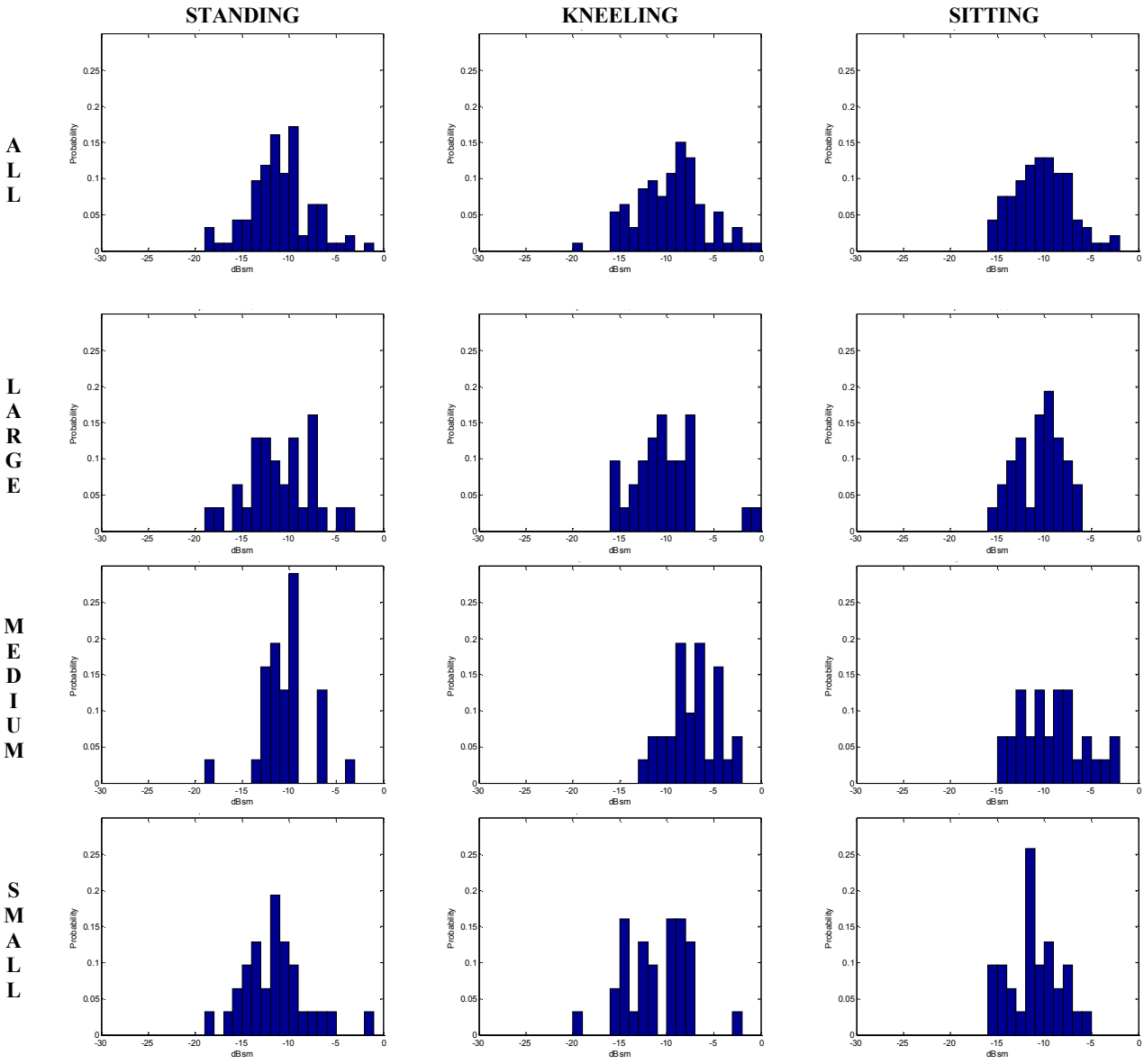

Figure 8. Experiment #1 RCS PDF of Dismounts versus Size and Non-Rifle Stances

These results are expected when we consider that the backscatter energy of the target is concentrated in one to a few resolutions cells for the coarser resolution case. For dismounts, a stronger value for the RCS at all aspect angles seems to result for the complex average of many scattering centers (and clutter) within a single resolution cell versus the average of a single scattering center (and clutter) within a resolution cell. This result is not true in general for all targets. We suspect that because the dismount has a characteristic Doppler spread due to an inability to remain perfectly still, target energy is naturally dispersed among many resolution cells. When the cell size is expanded, the Doppler energy is restored to a single cell along with the main return from the dismount (and additional clutter), yielding a larger RCS value. Despite the shift in the mean RCS values at the coarser resolution, the consistent PDF shape and spread in RCS values between resolutions indicate that the statistical target RCS characteristics of the dismount remain unchanged at the coarser resolution. The next section discusses this observation in more detail.

4.8. Dismount RCS Swerling Target Models

How a target's RCS fluctuates as a function of angle is important for setting algorithm probability of detection and false alarm thresholds. Figure 12 shows the Swerling target 1 and 2 models normalized against the overall dismount PDF for experiment #1 for both 4-inch and 3-foot resolutions. The Swerling 3 target model best fits the PDF of both resolutions.

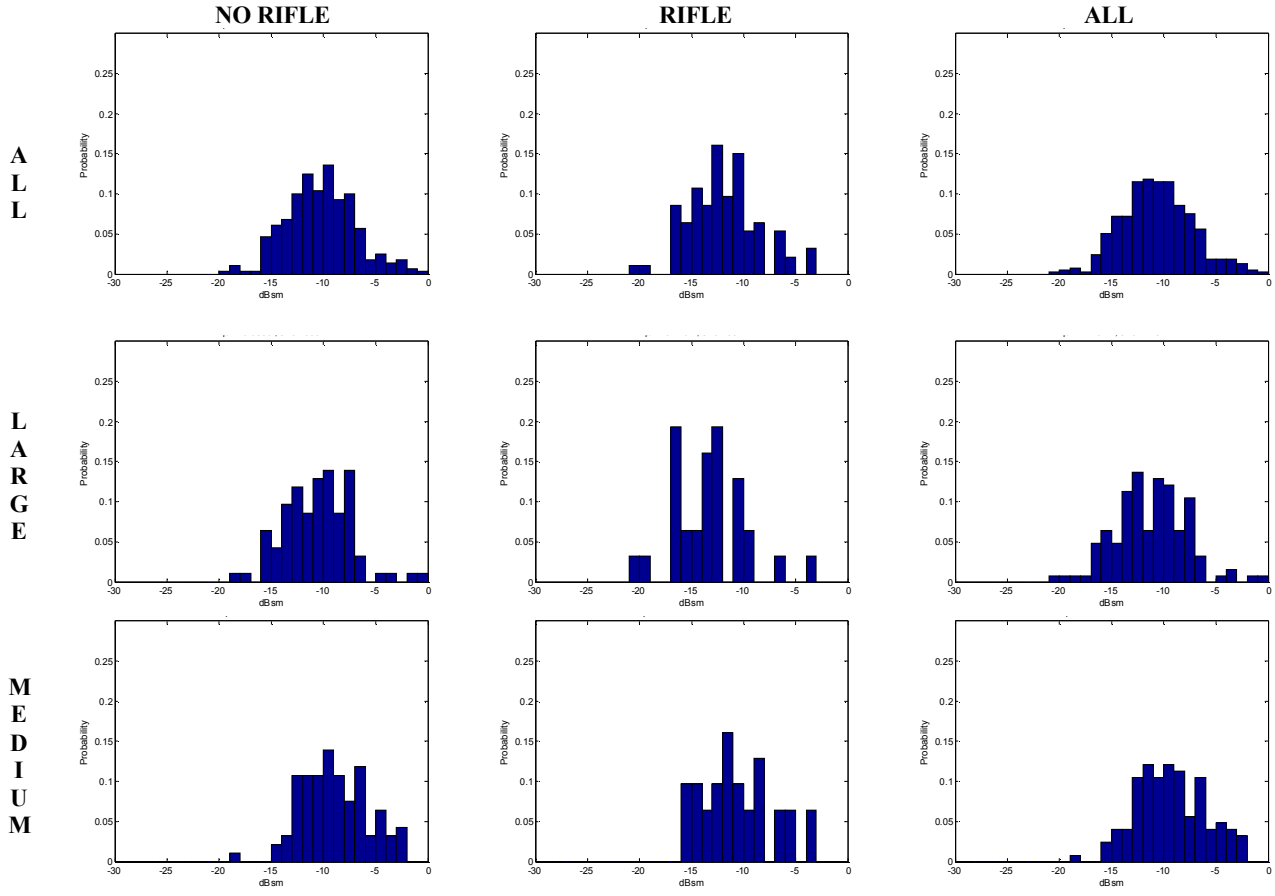

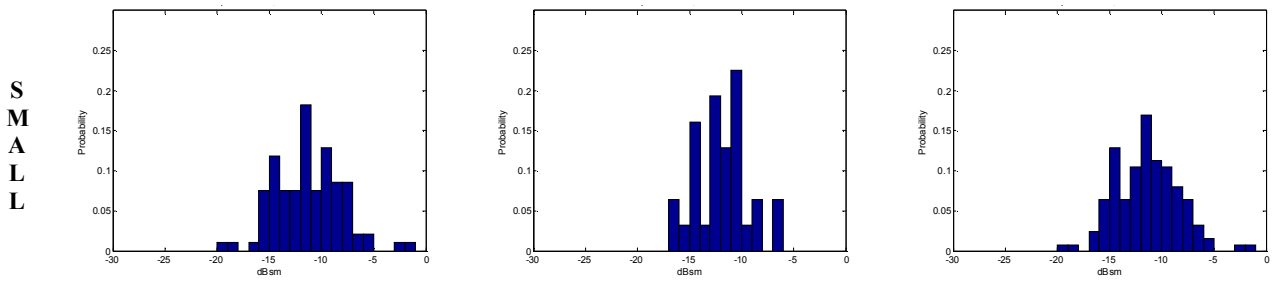

Figure 9. Experiment #1 RCS PDF of Dismounts versus Size and Device Stances

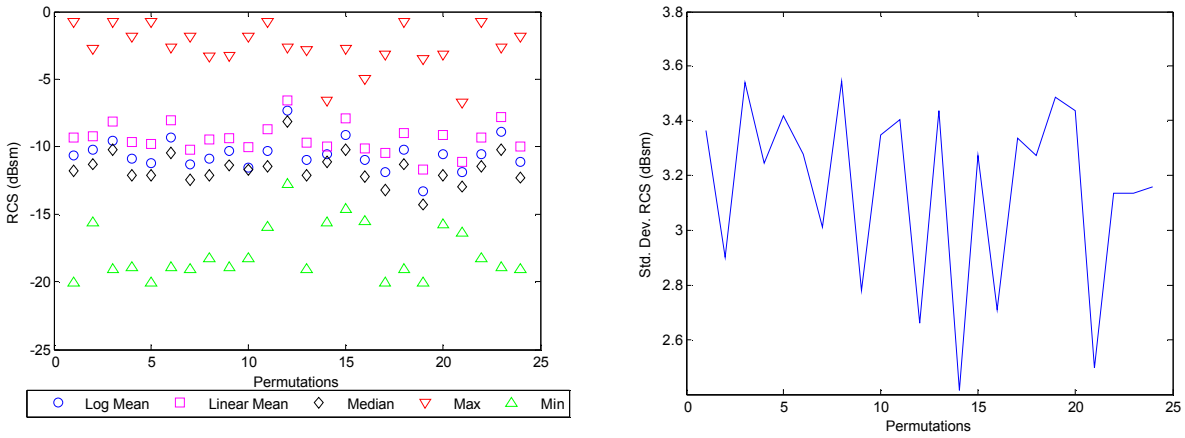

Permutations

1. All Sizes, Stances, Devices
2. Sitting, All Sizes
3. Kneeling, All Sizes
4. Standing, All Sizes
5. Large Person, All Stances, Devices
6. Medium Person, All Stances, Devices
7. Small Person, All Stances, Devices
8. Large Person, Standing
10. Small Person, Standing
11. Large Person, Kneeling on Both Knees
12. Medium Person, Kneeling on Haunches
13. Small Person, Kneeling on One Knee
14. Large Person, Sitting Legs Open
15. Medium Person, Sitting Legs Crossed
16. Small Person, Sitting Legs Crossed
17. Rifle, All Sizes
18. No Rifle, All Sizes, All Stances
19. Rifle, Side Carry, Large Person
20. Rifle, Front Carry, Medium Person
22. No Rifle, Large Person, All Stances
23. No Rifle, Medium Person, All Stances
24. No Rifle, Small Person, All Stances

Figure 10. Dismount RCS Statistical Values Across Stance, Size, and Device for Experiment #1

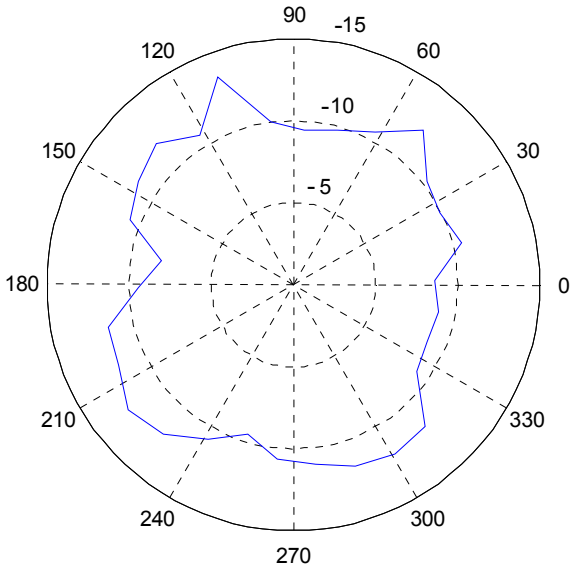

Figure 11. RCS Variation with Aspect Angle (All Stances, Sizes, and Devices) for Experiment #1

The Swerling model results are as expected. Although the target signature of a dismount is small in range and cross-range extent, the signature is comprised of multiple scatterers with one being dominant as seen in the SAR image chip in Figure 5. The resolution cell size impacts whether these scatterers are distinguishable across aspect or whether the scatterers are conglomerated and averaged into one cell. Irrespective of the resolution cell sizes analyzed, the dismount's single dominant scattering center from the torso, along with multiple scatterers from the limbs, yields Swerling 3 target characteristics. These results are consistent across dismount size, stance, device, pose, and polarization experimental RCS findings from our data sets.

We also note that the dismount distributions are chi-square, since that is the implicit assumption for the Swerling target 3 PDF which we have fitted to our data set. Furthermore, the degree of freedom for the chi-square distribution is 4 for the dismount distributions, since that many degrees of freedom are required for the Swerling 3 model.

Dogaru, et. al[12] suggest that the RCS fluctuations of an overweight dismount transition from Swerling 3 to 1 between lower and higher frequencies for a standing and kneeling human. The frequencies tested were 1.8 GHz and 2.5 GHz, and 0.5 GHz and 1 GHz for standing and kneeling at vertical polarization, respectively. The authors mention that the mean RCS value for different stances of a dismount are fairly similar across frequency from L through X-band from -4 to 0 dBsm. The independence of the mean RCS value across dismount stance or device is confirmed in our results at Ku-band. However, the Swerling target model is also seen to be independent. We additionally show that at Ku-band, the target is a Swerling 3 model for the resolution cell sizes analyzed. Our results are in line with those reported by Hersey, et al.[16] wherein their RCS distributions show Swerling 3 target characteristics for a walking human at X-band.

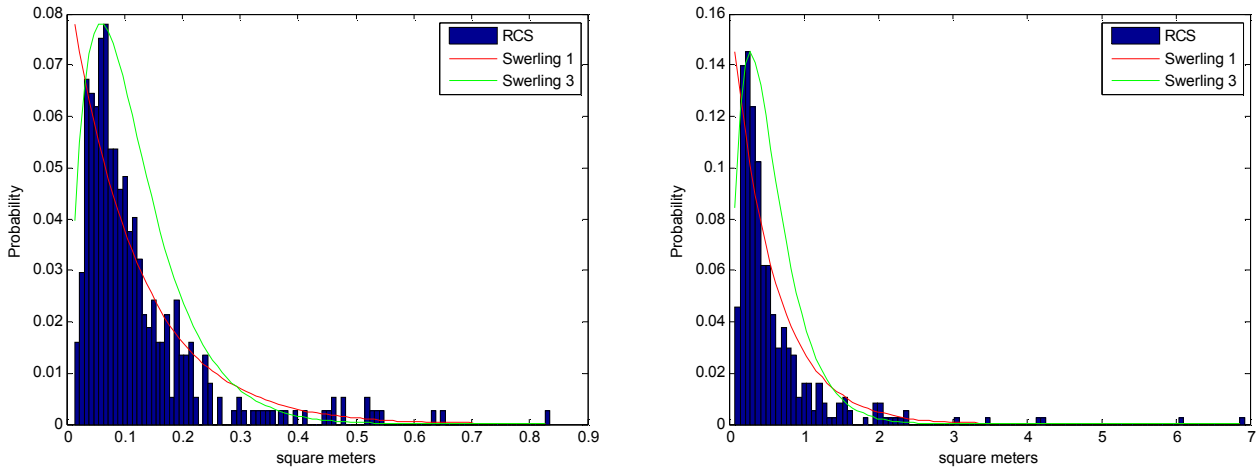

4-inch Resolution **3-foot Resolution**

Figure 12. Swerling Models Fitted to PDFs of Dismounts for Experiment #1

4.9. Effects of Grazing Angle and Clutter on Dismount RCS Distributions

If we compare experiment #2's distributions to those of experiment #1 in Figure 7, the distributions are not as defined for the latter case, as summarized by the standard deviation. This difference may be due to the fact that the experiment #2 collect was more limited (148 samples versus 360 and not a full-360-degree in aspect) such that the tales of the distribution were not fully defined. Despite this fact, the variation in clutter and grazing angle do not cause the general characteristics of the dismount distribution nor its statistics to radically change.

Simulations by Le and Dogaru

[**1** of RCS as a function of aspect and grazing angle suggest that the range of RCS values for our collected grazing angles is accurate. Our RCS distribution is skewed towards lower values in the case of 4-inch resolution. However, for 3-foot resolution, the distribution is centered near -5 dBsm and is in line with theoretical results. Furthermore, Le and Dogaru depict that RCS is generally lower as the grazing angle increases (except at front and back aspect angles of the dismount). This result is confirmed by our observations of the RCS variation as a function of grazing angle in Figure 13. The mean amount of change in RCS is comparable as well.

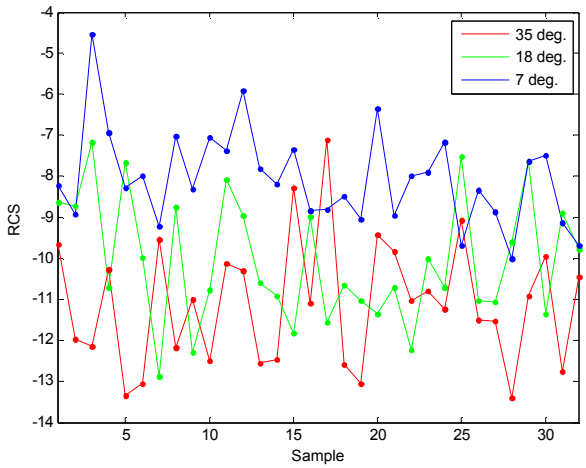

Figure 13. RCS Variation with Grazing Angle in Experiment #2 (dBsm)

4.10. Effects of Polarization on Dismount RCS Distributions

Simulation results[1] indicate that HH polarization should yield far greater RCS values at similar grazing angles, on the order of 4-5dBsm. This effect is not apparent in the data set of experiment #3, as evidenced by the distributions and

statistical values for VV at 35-degree grazing (squinted collect) in experiment #2, which are within 1 dBsm of each other (Figure 7). Given this discrepancy between experimental and theoretical results, granted with different clutter, subject, and collection scenarios between our experimental results, further investigation is necessary with a more controlled experiment to confirm or deny whether higher RCS truly results from HH versus VV polarization measured data.

4.11. Overall Dismount RCS Distributions

We refer to the overall statistics of dismounts at 4-inch and 3-foot resolution for all sizes, stances, devices, pose, polarization, and clutter of our three experiments in Figure 7. The geometric average RCS is -11 and -4.8 dBsm for 4-inch and 3-foot resolution, respectively. The dismounts exhibit a Swerling 3 target model. The overall RCS probability distribution range of values varied from about 0 to -20 dBsm and -12 to 7 dBsm for 4-inch and 3-foot resolutions, respectively. We conclude that a minimum detection threshold of -15.7 dBsm at 4-inch resolution and -7 dBsm at 3-foot resolution is required to achieve the likelihood of detecting a dismount 90% of the time. Similarly, we capture the dynamic range, noting that there is a 10% chance the dismount RCS will be above -9.2 dBsm or -0.5 dBsm for 4-inch and 3-foot resolution, respectively. The probability distributions of the dismounts validate these expectations.

From Le and Dogaru's results[1], we confirm that the range of RCS values for a fit man at Ku-band with VV polarization is spread between -2 and -14 dBsm across aspect and -9 to 4 for HH polarization based on their Xpatch simulations for the grazing angles we studied. Their mean values are higher than our measurements overall at 4-inch resolution, but more consistent at 3-foot resolution. For instance, they report that the mean and standard deviation of the RCS should be near -6 and 2.3dBsm, respectively, at 18-degree grazing, VV polarization. The CDF median (a more accurate metric for measured data) is at least 6 dBsm lower and the standard deviation is 1dBsm larger for our results at 4-inch resolution as compared to the Xpatch simulations. Our 3-foot resolution results are more consistent in terms of the median, with only the 1 dBsm difference in the standard deviation. We note that finding the peak RCS in target detection schemes usually implies that the full target is within a single resolution cell, which is why our 4-inch resolution results are possibly so different from the Xpatch values. The subtle discrepancy between Xpatch and our 3-foot resolution results may be due in part to the clothing and clutter background of the subjects in our experimental data sets as well. Clothing was not modeled at all in the simulation. Furthermore, although ARL used a rough ground plane in their study, they also stress the importance of an appropriate ground surface model for simulation. The discrepancy is not statistically significant, however. With respect to our 4-inch resolution results, Cordaro[**8**] has independently verified an experimental RCS on the order of -11 dBsm for dismounts in an unpublished GMTI study from 2006. Walking dismounts had a mean RCS of about -11.5 dBsm at 27-degree grazing for Ka-band, with all other parameters being the same. This value is 3.7dBsm lower than that reported[1] for a stationary dismount at Ka-band. A resolution, ground plane, or clothing discrepancy may be at play here as well.

5. CONCLUSIONS

We examined the RCS probability distributions of different sized humans in various stances, across aspect and elevation angle, polarization, resolution, and clutter from three experimental studies. Geometric mean, standard deviation, median, and arithmetic mean were consistent irrespective of dismount size, stance, pose, polarization, or clutter background. At 3-foot resolution, where the target return of the dismount is comprised by one or a few resolution cells, the RCS value averages were roughly 6-7 dBsm stronger than for 4-inch resolution data. The target RCS fluctuations across look angle were found to be characteristic of a Swerling 3 target for both resolutions. Detection thresholds for a 90% probability of detection and RCS values for which the dismount RCS had a 10% probability of exceeding that value were determined. Thus, expectations for radar algorithm design and performance for dismount detection can be appropriately established. Good agreement was noted between theoretical and experimental observations that dismount RCS decreases with grazing angle, is independent of dismount stance and size, and is near theoretical mean and standard deviations (within modeling, clutter, and statistical error) at 3-foot resolution. Discrepancies of 6 dBsm between electromagnetic modeling simulations and experimental results occur at 4-inch resolution due to spreading of the Doppler energy of the dismount over multiple resolution cells at finer resolutions for a peak detection assumption. Another key discrepancy between theoretical and empirical data is that HH polarization yields 4-5 dBsm higher RCS returns than VV. Limited empirical data did not show this advantage and further experimental study of RCS as a function of polarization and pose for different clutter types is recommended before considering radar design choices towards a particular type of polarization.

ACKNOWLEDGMENTS

This report was funded by General Atomics Aeronautical Systems, Inc. (ASI) Reconnaissance Systems Group (RSG). The authors would also like to thank the Sandia National Laboratories (SNL) for kindly allowing us to use the human personnel experimental data set acquired in 2004 with their Ku-band test bed radar system. Finally, this study would not have been possible without the coordination and participation of ground teams at General Atomics and Sandia for additional collects in 2011 with their Ku-band radar systems.

Sandia National Laboratories is a multi-program laboratory managed and operated by Sandia Corporation, a wholly owned subsidiary of Lockheed Martin Corporation, for the U.S. Department of Energy's National Nuclear Security Administration under contract DE-AC04-94AL85000.

GA-ASI, an affiliate of privately held General Atomics, is a leading manufacturer of Unmanned Aircraft Systems (UAS), tactical reconnaissance radars, and surveillance systems, including the Predator® UAS-series and Lynx radar.

REFERENCES

[1] C. Le and T. Dogaru, "Numerical modeling of the airborne radar signature of dismount personnel in the UHF-, L-, Ku-, and Ka-bands," *Army Research Laboratory Report*, ARL-TR-4336, Dec. 2007.

[2] T. Dogaru, L. Nguyen, and C. Le, "Computer models of the human body signature for sensing through the wall radar applications," *Army Research Laboratory Report*, ARL-TR-4290, Sept. 2007.

[3] M. Otero, "Application of a continuous wave radar for human gait recognition," *Proceedings of the SPIE 2005 Defense and Security Symposium, Conference on Signal Processing, Sensor Fusion, and Target Recognition XIV*, Orlando, FL, vol. 5809, pp. 538-548, Mar. 2005.

[4] T. Dogaru, C. Le, and G. Kirose, "Time-Frequency Analysis of a Moving Human Doppler Signature," *Army Research Laboratory Report*, ARL-TR-4728, Feb. 2009.

[5] S. R. Stratton and R. L. Bender, "Radar cross-section (RCS) measurements of a dismount with rocket-propelled grenade (RPG) launcher at Ka-band," *Army Research Laboratory Report*, ARL-TR-3855, July 2006.

[6] R. K. Hersey, W. L. Melvin, E. Culpepper, "Dismount modeling and detection from small aperture moving radar platforms," *IEEE Radar Conference*, Rome, Italy, 2008.

[7] P. Swerling, "Probability of detection for fluctuating targets," *IRE Transactions on Information Theory*, vol. 6, issue 2, pp. 269-308, 1960.

[8] T. Cordaro, "Preliminary results from the Ka-band endoclutter tests," *Sandia National Laboratories Presentation*, Sept. 12, 2006.